Proceedings ASME Turbo Expo 2005
Power for Land, Sea, and Air
June 6-9, 2005, Reno, NV, U.S.A.

GT2005-68704

EXPERIMENTAL CHARACTERIZATION OF FILM-COOLING EFFECTIVENESS NEAR COMBUSTOR DILUTION HOLES

J. J. Scrittore and K. A. Thole
Mechanical Engineering Department
Virginia Polytechnic Institute and State University
Blacksburg, VA 24061

S. W. Burd
Pratt & Whitney
United Technologies
East Hartford, CT 06108

ABSTRACT

Cooling combustor chambers for gas turbine engines is challenging, given the complex flow and thermal fields inherent to these modules. This complexity, in part, arises from the interaction of high-momentum dilution jets required to mix the fuel with film cooling jets that are intended to cool the combustor walls. This paper discusses the experimental results from a combustor simulator tested in a low-speed wind tunnel that includes both the dilution jets and film-cooling jets. The specific purpose of this study is to evaluate the influence that the dilution jets has on the film-cooling effectiveness. Infrared thermography was used to measure surface temperatures along a low thermal conductivity plate to quantify the adiabatic effectiveness from an array of film cooling holes with the presence of dilution holes. To further understand the flow phenomena, thermocouple probes and laser Doppler velocimetry were used to measure the thermal and flow fields, respectively. Parametric experiments indicate that the film cooling flow is disrupted along the combustor walls in the vicinity of the high-momentum dilution jets. In fact, a significant penalty in cooling effectiveness of the combustor is observed with increased dilution jet penetration.

INTRODUCTION

Firing temperatures of gas turbine combustors are higher than ever as the demand for higher output gas temperatures increase. The ability to effectively cool the chamber walls of gas turbine combustors is important to insure a stable combustion system and the required durability. As such, it is important to identify hot-spots that may occur along the combustor walls. It is also essential to identify flow features that reduce the cooling effectiveness of the combustor liner.

The flow and thermal fields in a gas-turbine combustor are some of the most important and complex physical processes in a gas-turbine engine. A typical gas turbine aero-engine employs an annular combustor with dilution holes and film cooling holes. The dilution jets serve to increase mixing of the fuel and air and insure that there is efficient combustion and quality of the combustion gases exiting the combustor. As such, high jet penetration may be desired to promote high levels of turbulence to assist in the mixing process. The introduction of cooling air along the combustor chamber walls serve to isolate the walls from the hot combustor gases and provide the heat transfer required to cool the walls. As such, low film-cooling jet penetration with little mixing may also be desired. Irrespective of these objectives, the dilution and cooling air flows remain constrained by the overall combustor air budget making it important to understand these trades.

To evaluate the cooling that might be expected in a typical combustor of an aero-engine, a large-scale facility was developed to simulate typical combustor flows. The study presented in this paper does not include the reacting flow thereby effects attributed to the heat release due to combustion are not represented in this study. From these large scale tests, however, it is possible to understand the effects on combustor liner cooling.

The objective for the work reported in this paper was to quantify the film-cooling effectiveness in the vicinity of dilution jets for different conditions. Typically, combustors have multi-row film-cooling holes that are closely spaced. Moreover, the film-cooling blowing ratios are typically higher than those presented in most of the open literature. This study is unique because it simulates the combined film-cooling and dilution jets and was completed for realistic blowing ratios. After describing the development of the combustor simulator facility, this paper describes measured adiabatic wall temperatures to quantify cooling effectiveness. Flow and thermal fields were measured near the dilution jets to gain better understanding of how the flow is behaving in this region. This paper concentrates on how the liner cooling and the flow and thermal fields are sensitive to the blowing ratios of these different jets.

NOMENCLATURE

ALP	air loading parameter, $ALP = P_o^{1.75} A_{ref} D_{ref}^{0.75} e^{T/300} \big/ \dot{m}$, Lefebvre [1]
A_{ref}	reference combustor area
d	film cooling hole diameter
D	dilution hole diameters
D_{ref}	reference diameter
H_{in}	combustor inlet height
I	momentum flux ratio, $I = \rho U^2 \big/ \rho_\infty U_\infty^2$
L	film cooling/dilution hole length, combustor simulator length
m	mass flowrate
M	mass flux ratio, $M = \rho_c U_c / \rho_\infty U_\infty$
P	vane pitch
P_0	total pressure
S_s, S_p	streamwise, pitchwise film cooling hole spacing
T	temperature
TL	turbulence level, $TL = \sqrt{0.33\left((u_{rms}^2 + v_{rms}^2 + w_{rms}^2)\right)} \big/ u_{in}$
Tu	turbulence intensity, $Ti = \sqrt{0.33\left(u_{rms}^2 + v_{rms}^2 + w_{rms}^2\right)} \big/ \sqrt{u^2 + v^2 + w^2}$
u, v, w	local, mean velocity components
X, Y, Z	coordinate system shown in Figure 2a
U_{in}	combustor inlet velocity
W	combustor inlet width

Greek

ρ	density
ν	kinematic viscosity
θ	non-dimensional temperature, $\theta = (T_\infty - T)/(T_\infty - T_c)$
η	adiabatic effectiveness, $\eta = (T_\infty - T_{adiabatic})/(T_\infty - T_c)$

Subscripts

ave	spatial average
rms	root mean square
∞	freestream conditions (primary flow)
c	coolant conditions (secondary flow)
d	dilution flow
fc	film-cooling flow

RELEVANT PAST STUDIES

Many experimental studies have been reported in the open literature documenting both experimental and computational data for model combustor flows. The large number prevents a full discussion of all of the results in our paper, but rather a small subset will be discussed that is relevant to cooling methods for combustor liners. Cooling methods for combustor liners consist of the following: film-cooling (also referred to as effusion cooling), slot cooling, backside impingement, and backside pin fin cooling. Both the film-cooling and slot cooling are highly susceptible to any effects that the dilution jets may cause such as increased mixing and interruption of the cooling flow along the liner.

Most combustor film-cooling patterns consist of a closely spaced array of holes, also known as full-coverage film-cooling, which has been studied by a number of investigators. Sasaki et al. [2] examined if it were possible to use a superposition method with full-coverage film-cooling. They found that, in fact, there was an additive nature of multi-row film-cooling that allowed the use of the superposition method. A series of papers by Andrews et al. [3 and 4] have compared the influence of cooling hole size and pitch through a number of experimental studies. In combustor designs, the amount of coolant flow per surface area must be considered in the design of the cooling hole diameter to insure that the hole loss is of similar levels as the pressure loss across the combustor. From this study, larger pressure losses generally occur for smaller cooling holes than for larger cooling holes at a given cooling flux. The discharge coefficients of any hole pattern, however, are a function of the hole geometry and the aerodynamics to which the holes are exposed. It is necessary to supply the flow at an adequate pressure drop and quantity to prevent any ingestion of hot gas into the cooling holes. Barringer et al. [5] found that film-cooling hole discharge coefficients depend on the coolant to freestream density ratio and the number of rows of holes in the array. Their results indicated that increasing the number of rows slightly increased the discharge coefficient due to the increased film layer causing a reduction in the resistance to the film-cooling flow. Gritsch et al. [6] found that for a 30° inclined, cylindrical film-cooling hole, the overall discharge coefficient of any flow configuration can be predicted if the pressure ratio across the hole and the hole jet-to-internal and external crossflow momentum flux ratios are known. These results show the influence of external crossflow on discharge coefficients. Andrews et al. [4] found that for the same hole pitch and coolant flow, cooling effectiveness increased nearly linearly with cooling hole diameter and the heat transfer coefficients decreased nearly linearly with cooling hole diameter.

Three studies have looked at a disruption of a film-cooling layer by a larger normal jet that include Odgers and Son [7], Button [8], and Martiny et al. [9]. Odgers and Son [7] found that when a normal jet, such as a dilution jet, was injected into a film-cooling layer at $I_d < 20$, the net effect on the film-cooling efficiency depended upon the dynamic pressure ratio of the jet relative to the hot mainstream gas (note this is analogous to momentum flux ratio). If the dynamic pressure ratio was below unity, there was a net benefit on film-cooling efficiency. If, however, the ratio was larger than unity, as most combustors are designed, there was a net reduction on effectiveness.

Button [8] evaluated the effectiveness for a slot alone, a jet alone (I_d = 0.25 to 4), and the combined slot and jet. In all of the cases they considered, the combined slot and jet indicated lower effectiveness levels as compared to the slot alone. Martiny, et al. [9] performed experiments whereby slot film-cooling was interrupted by a single large dilution jet at I_d = 7 and 10. They also determined that the film-cooling lifted off the wall just downstream of the dilution jet leading to weaker film-cooling coverage and increased heat transfer coefficients in this area. Their measurements indicated a reduction in the adiabatic effectiveness levels by as much as 25% in the area just downstream of the jet injection location. Similar to Odgers and Son, they found that the effect was more dramatic with higher jet momentum flux ratios.

As others have shown, the turbulence levels in a combustor resulting from the dilution jet injection are relatively high. In a related paper with a geometry similar to that reported in our paper, Vakil and Thole [10] reported measured turbulence

levels that were extremely high throughout the combustor as well as highly anisotropic. Moreover, the thermal field measurements of the film-cooling layer downstream of the dilution jet injection indicated a much thicker layer relative to upstream of the dilution jets. This vertical spreading of the coolant into the hot gas path was attributed to the mixing caused by the very high turbulence levels.

In summary, there is little data presented in the literature with a realistic cooling configuration for a gas turbine combustor. While there is an abundance of film-cooling literature, much of this data is not applicable because of the high blowing ratios required for most aero-engine combustors, the densely spaced cooling holes and the interaction that the cooling has with the large dilution jets. Our study presents data that is of interest to designers and modelers who develop combustor cooling methods.

FACILITIES AND MEASUREMENT METHODS

The focus of this study was to obtain highly resolved surface measurements of adiabatic effectiveness for a realistic combustor cooling design. To achieve good spatial resolution, it is beneficial to use large scale models while matching the relevant non-dimensional parameters. The primary measurement techniques used was an infrared camera, in which surface temperatures could be deduced, a laser Doppler velocimeter to quantify the flow field, and a thermocouple rake to quantify the thermal field. This section describes the experimental facility used to achieve these measurements as well as the instrumentation that was used followed by estimates of measurement uncertainty.

Experimental Facilities

The development of the combustor simulator used in our study was previously described by Barringer et al. [5] and Vakil and Thole [10]. The geometric scaling factor for the combustor was 9X, which permitted good measurement resolution in the experiments, and was matched to that of a linear turbine vane cascade that was pre-existing. Other than performing the measurements in an actual operating engine, it is not feasible to have a measurement environment with representative turbine engine conditions. In designing this combustor simulator, the parameters chosen for a prototypical combustor for aircraft applications included the following: i) a combustor exit velocity that insured the needed inlet Reynolds number for the downstream turbine section; ii) coolant-to-mainstream momentum flux ratios of the liner cooling holes and the dilution holes; and iii) scaled geometric features of a combustor including the film-cooling staggered hole pattern and dilution hole size and placement. Note that the parameters for the prototypical engine combustor are for actual running (hot) operating conditions. The air loading parameter (ALP defined in the nomenclature) for the wind tunnel design was 0.40×10^{-4}.

Figure 1 illustrates the wind tunnel containing the combustor simulator and turbine vane test sections. Downstream of a primary heat exchanger is a transition section that divides the flow into three channels that include a heated

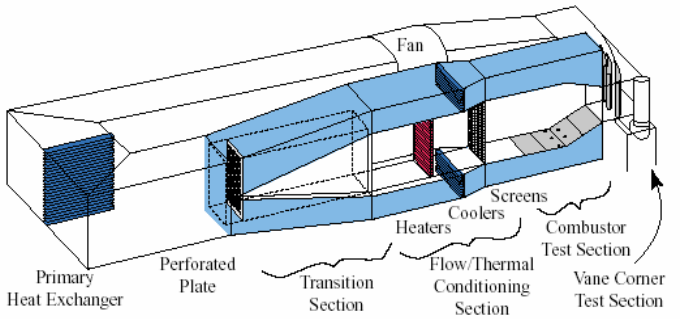

Figure 1. Illustration of the wind tunnel facilities used for combustor simulator experiments.

primary channel, representing the main gas path (center arrows), and two symmetric secondary channels (outer arrows), representing the coolant flow path. Within the transition section of the primary channel, the flow immediately passes through a perforated plate that provides the necessary pressure drop to control the flow splits between the primary and secondary passages. At a distance 2 m downstream of the perforated plate, the flow passes through a bank of heaters followed by a series of screens and flow straighteners. The heater section comprises three individually controlled banks of electrically powered, finned bars supplying a maximum total heat addition of 55 kW. Downstream of the flow straighteners, the heated primary flow enters the combustor simulator. In the combustor simulator, secondary coolant flow is injected into the primary flow passage through cooling panels for the combustor liner and through dilution holes. In addition, the flow is accelerated prior to entering the turbine section. In addition to heat being removed from the flow by a primary heat exchanger, the flow in the secondary passages must go through a second heat exchanger to further reduce the coolant flow temperature. The flow in the secondary passages is then directed into a large plenum that supplies combustor liner coolant and dilution flow.

The cooling hole pattern in the panels is illustrated in Figures 2a-2b. To insure representative coolant flow splits among the three liner panels and dilution row, separate supply chambers with adjustable shutters were used. The mass flow exiting the film-cooling holes was set by applying the appropriate pressure ratio between the supply plenum and the exit static pressure. Using previously documented discharge coefficients for this particular cooling hole configuration (Barringer et al. [5]), the mass flows through the panels were determined. The dilution holes were spaced two hole diameters apart. The mass flows exiting the dilution holes were set by directly measuring the velocity through the use of a pitot probe installed at the exit of the dilution hole.

The combustor simulator begins at the start of the first panel, as illustrated in Figure 2a**.** The cross-sectional area of the simulator at this location is 1 m in height (H_{in}) and 1.1 m in width (W). At the exit of the simulator, the cross-sectional area is 0.55 m in height and remained 1.1 m in width giving an inlet to exit area ratio of 1.8. The width was to allow for a span that was slightly greater than a turbine sector while the height was matched to that of the radial extent of a first vane. The area ratio was matched to a non-dimensional acceleration parameter through an aeroengine combustor.

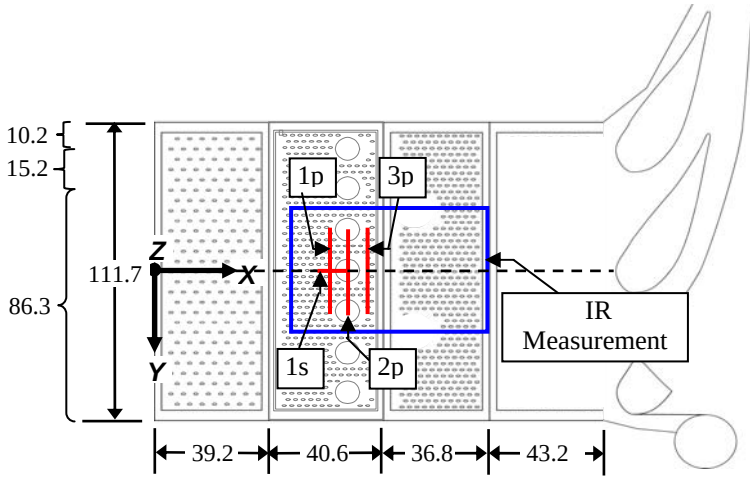

Figure 2a. Layout and measurements planes for the combustor simulator (dimensions in cm).

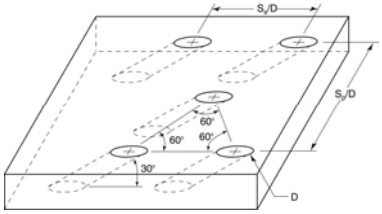

	S_p/d	S_s/d
Panel 1	10.1	5.8
Panel 2	6.1	3.5
Panel 3	6.1	3.5

Figure 2b. Illustration and description of cooling hole arrangement for liners.

The liners for the combustor simulator were a streamwise series of three film-cooled panels that started 2.7 vane chords (1.6 m) upstream of the turbine test section. The lengths of the first two panels were 39 cm and 41 cm while the third panel was 37 cm. The panels extended across the full width of the test section, which was slightly greater than a scaled turbine sector. The first two panels were flat to maintain a constant cross-sectional area while the following two panels were inclined at 15.7° to give the required area contraction. As shown in Figure 2a, there is a region on the third panel in which there were no film-cooling holes. Previously, there was a second row of dilution holes, but in this study second row of dilution holes was sealed off to isolate the effects on cooling by a single row, to prevent communication between rows and to eliminate the blockage effects of the aft row. Moreover, given facility flow-loss capacity, the limitation of the open dilution flow to one row allowed a dilution ratio $I_d = 125$ to be achieved and investigated in this study. In addition, the first dilution row was fabricated in the second panel to which a developed, fairly uninterrupted cooling flow was provided. Measurements were also facilitated by the fact that the combustor walls were parallel to the opposing walls in this section of the combustor simulator. The panels were constructed of 1.27 cm thick urethane foam with a low thermal conductivity (k = 0.037 W/mK) to allow for adiabatic surface temperature measurements. The dense matrices of film-cooling and dilution holes were cut into the urethane foam using a water jet.

One parameter that is not representative is the coolant-to-mainstream density ratios, which are typically quite high. Typical operating conditions were near atmospheric pressure with flow temperatures for the mainstream of 50˚C and a coolant flow temperature of 20˚C. Although the density ratios were not matched, the jet-to-mainstream momentum flux ratios and percentage of mass flow addition by both the film-cooling and dilution holes were representative. The momentum flux ratio is the parameter that most affects mixing characteristics of jets in cross-flow at high momentum flux ratios. Holdeman [12] simulated a non-reacting gas turbine combustion chamber by conducting computations and experiments on the mixing of single, double, and opposed rows of dilution jets with an isothermal or variable temperature mainstream in a confined subsonic crossflow. The principle finding from the investigation was that the momentum flux ratio of the jets dictated the exit velocity and temperature profiles. The results from the cases involving opposed-rows of jets revealed that for in-line jets the two streams mixed very rapidly and that the effective mixing height was half the duct height for equal momentum flux ratios on both sides. The cooling hole patterns, shown in Figure 2b, were configured in equilateral triangles and spaced evenly across the surface. The diameter of the cooling holes was 0.76 cm giving an L/d = 3.3.

The dilution hole diameters were designed to insure the percent mass addition of the dilution fluid and coolant-to-mainstream momentum flux ratios were representative of that in an engine. There are seven dilution holes in a row, evenly spaced with the center hole being aligned with the center of the simulator (and also the vane stagnation). The dilution row is located at 43% of the combustor length (0.67 m) downstream of the start of the panels. The dilution holes have a diameter that is 7.6 cm. The supply chamber for the dilution flow was required to be some distance from the hole exits giving an L/D ratio of 5. The combustor simulator is symmetric about the vertical mid-span meaning that for each row the dilution holes were aligned with one another in the pitchwise and streamwise directions.

For the cases presented in this paper, between 38% and 45% of the total flow was directed through the primary passage of the combustor simulator while the remaining flow is directed through the secondary coolant passages for the liner coolant and dilution holes. Of the total cooling flow, 50% is injected through the film-cooling holes and 50% is injected through the dilution holes. The density ratio for all of the cases investigated was 1.08 (jet-to-mainstream) while the flow accelerated to nearly 2.5 times the inlet velocity through the combustor simulator as a result of the mass flow addition and contraction ratio. These flow conditions resulted in an exit Reynolds number for the combustor of 2.1×10^5.

Instrumentation and Measurement Uncertainty

A Flir Systems P20 infrared camera was used to take measurements of the combustor liner panels to calculate the adiabatic effectiveness at the liner surface. The camera captured the temperature of the surface at each image pixel location by measuring the total heat flux emitted from the black painted foam liner panels. Two surface type E thermocouples measuring temperatures at the surface of the panel were used to calibrate the images to assure that the correct surface emissivity and ambient temperatures were being used to report the actual surface temperatures. Five pictures were averaged at each image location to reduce uncertainty in the measurements.

The large scale of the combustor permitted the infrared camera to be mounted in the primary path of the combustor simulator 0.5 m from the liner wall upstream of the dilution holes. The close proximity of the camera to the combustor wall allowed good spatial resolution of less than 1 mm, with a maximum image size of 700 square centimeters. However, the non-orthogonal camera angles and the exposure of the camera to the hot primary flow required additional steps in the infrared image calibration process in which the images were transformed into a correctly dimensioned image.

Thermocouples were used in monitoring inlet and coolant temperatures as well as taking the thermal fields within the combustor. All of the temperature measurements were made using 30-gage, type E thermocouples that were connected to a data acquisition system through 20-gage thermocouple extension wire. All of the thermocouples used in this study were made using an argon-gas thermocouple welder that resulted in spherical beads ranging in diameter from a minimum of approximately 0.8 mm to a maximum of 1 mm. The thermal fields were taken using a twenty-one probe thermocouple rake. The rake spanned a total distance of 10.2 cm with thermocouples evenly spaced every 5.1 mm. Each thermocouple probe on the rake consisted of a 5.1 cm long, 2.5 mm outer diameter aluminum casing that encapsulated the thermocouple wire. The approximate flow blockage was shown to have no effect on the measured thermal field. Each thermocouple bead is fixed approximately 6.4 mm from the end of the aluminum shaft in order to minimize heat conduction effects from the aluminum rod to the thermocouple.

Velocities were measured using a two and a three-component laser Doppler velocimeter (LDV). The flow was seeded with olive oil particles that were nominally 1 μm in diameter. The probability of obtaining a sample was proportional to the speed of the flow; therefore, statistical particle bias corrections were applied to the data by weighting eachsample based on the residence time in the probe volume.

In taking flow plane measurements that were aligned with the flow direction, a single fiber optic LDV probe capable of measuring two-components was used. To allow the measurement volume of the probes to reach mid-pitch of the combustor simulator, data was taken with a 750 mm focusing lens equipped with a 2.6 magnification beam expander. This set-up had a measurement volume of 73 μm in diameter and 1.3 mm in length. The plane was acquired with the probe perpendicular to the outer wall surface. This allowed for the direct measurement of the local streamwise velocity component, *u*. However, in order to take measurements near the surface of the liner panel, the probe was slightly tilted at 8.8˚, whereby there was little effect on the true vertical component measurements.

For the measurements taken in the cross-stream direction where three-component velocity measurements were made, two separate fiber optic probes were used. This set-up also used a 2.6 magnification beam expander along with a 750 mm focusing lens. Using these two probes, the measurements were conducted through a non-orthogonal set-up requiring the velocity components to be transformed into the true components. Furthermore, as with the single LDV probe measurements, a tilt was applied to both probes to allow for near-wall measurements. To insure a single beam crossing, both probes were turned 14˚ towards each other off of the cross-stream direction while the vertical tilt angle was set to 8.8˚. The nominal sampling time for each measurement location was 20 seconds whereby 10,000 data points were acquired for each component.

The partial derivative and sequential perturbation methods, described by Moffat [11], were used to estimate the uncertainties of the measured values. Precision uncertainties were calculated based on a 95% confidence interval using the deviation of six measurement sets of IR camera images with each set consisting of five images. The precision uncertainty of the measurements was ±0.088°C. The bias uncertainty was ±0.44°C based on the calibration of the image. The bias uncertainty of the thermocouples was ±0.2°C. The total uncertainty was then calculated as ±0.47°C for the images and ±0.22°C for the thermocouples. Uncertainty in effectiveness, η, was found based on the partial derivative of η with respect to each temperature in the definition and the total uncertainty in the measurements. An uncertainty of $\partial\eta = \pm 0.017$ at $\eta = 0.4$ and $\partial\eta = \pm 0.019$ at $\eta = 1.0$ were calculated. The precision uncertainty for the highest streamwise velocities was 0.79% while the bias uncertainty for the mean velocity measurements was 1%. The bias and precision uncertainties on the thermal field values was ±0.2 and ±0.4, respectively, giving an uncertainty of ±0.021 at $\theta = 0.9$ and ±0.020 at $\theta = 0.3$.

MEASURED SURFACE EFFECTIVENESS, FLOW AND THERMAL FIELD RESULTS

The measurements made in this study included adiabatic wall temperature measurements and flow and thermal fields. The adiabatic wall temperatures were resolved over the entire combustor liner surface. Flow and thermal field measurements were made at four planes near the mid-pitch dilution hole as shown in Figure 2a. These locations were chosen to illustrate the effect of the dilution and film cooling interaction on the flow and thermal fields and the effects of different momentum flux ratios on cooling effectiveness. It should be noted that the combustor simulator area remains constant at all of the measurement planes in this study. The measurement locations include the following: i) a pitchwise plane 0.75 dilution hole diameters upstream of the mid-pitch dilution hole whereby the film cooling thermal field can be quantified (1p), ii) at the dilution jet centerline to capture effects in the core of the high momentum dilution jet (2p), iii) 0.75 dilution hole diameters downstream of the dilution jet (3p), and iv) a streamwise plane at mid-pitch beginning 1.5 dilution hole diameters upstream of the dilution hole (1s). The flow conditions that were set are summarized in Table 1 for each of the film-cooling flows and dilution flows. Note that two different film-cooling flows and two different dilution flows were studied. The momentum flux ratios are defined using the freestream velocity at the start of the combustor simulator (first panel). The density ratio for all of the tests was nearly unity (1.08).

Adiabatic Effectiveness Measurements

Adiabatic surface temperature measurements were made in a region extending one dilution hole pitch on either side of the

TABLE 1. MOMENTUM FLUX RATIONS FOR FILM-COOLING AND DILUTION JETS

Configuration	Film Cooling, *I*	Dilution, *I*
Case #1	25	125
Case #2	12	60
Case #3	25	60
Case #4	12	125

downstream vane stagnation point. This region extended 28% of the width of the combustor simulator. The streamwise extent of this region was chosen to quantify the development of the film-cooling upstream of the dilution jets as well as in the near-jet region. Three dilution jets were included in this region, but it should be noted that there were seven dilution jets across the entire width of the combustor simulator (one vane sector). This was done to show that periodicity had been achieved.

Figure 3 shows the adiabatic effectiveness contours for each of the four test cases. For these cases, the nature of the contours shows little difference yet the flow conditions are quite different. Upstream of the dilution jets, it is clearly seen that there are high temperature streaks between the staggered rows of film-cooling holes, which indicate $\eta = 0.4$ values. These distinct jets upstream of the dilution jets are in stark contrast to what occurs downstream of the dilution jets where the jets become more merged indicating nearly an isothermal wall. This downstream phenomenon can be attributed to the high turbulence levels created by the dilution jets. The high turbulence serves to mix out the film-cooling jets and thereby providing better wall coverage.

The cooling performance depends upon where the rows of film-cooling holes intersect the dilution holes. Our results indicate that just upstream of the dilution jet the worst condition occurs at the center hole in which a row of film-cooling jets is directly aligned with the centerline of a dilution jet. Hot streaks surround the center dilution hole relative to the outer two dilution holes, where for the other two dilution jets the film-cooling jets are not directly aligned with the centerline of the dilution jets. In all cases, however, it does appear that there is some coolant that surrounds the dilution hole even though the presence of the film-cooling holes is quite sparse.

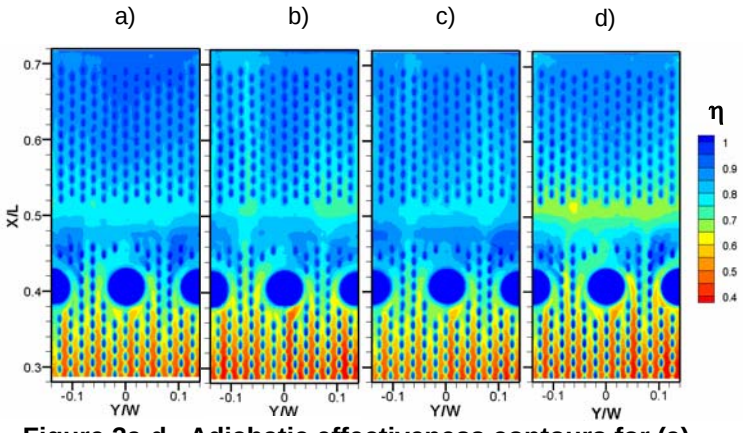

Figure 3a-d. Adiabatic effectiveness contours for (a) configuration 1, (b) configuration 2, (c) configuration 3, and (d) configuration 4.

Downstream of the dilution holes, there is an agglomeration of cooler fluid which has been convected around the dilution jets as a result of the vortices that have developed. Furthermore, the start of the contraction promotes better cooling at this location just downstream of the dilution holes. On the cooling panel downstream of the dilution holes, it is obvious that there is a lack of cooling where the film-cooling holes are not present, but there is some effect of the dilution jets impacting the downstream wall as well. This flow behavior and the impact the dilution jets have on cooling are described in more detail in the subsequent sections and paragraphs. Other specific conclusions from Figure 3 are that (1) the streaks around the dilution holes are more substantial in surface coverage downstream and between the large holes at the lower cooling momentum flux ratio, (2) cooling effectiveness values are lower downstream of the dilution holes for the higher dilution I_d case and (3) cooling effectiveness is lower in the region between panels 2 and 3 with $I_{fc} = 12$ (as represented by the "green" areas in the contour plots around X/L = 0.5). The discussion that follows provides more details regarding these observations.

Lateral averages of adiabatic effectiveness for the four cases given in Figure 3 are shown in Figure 4. It was found that the best cooling upstream of the dilution holes occurs when the film-cooling is set to the higher blowing ratio (cases 1 and 3) relative to the lower blowing ratio (cases 2 and 4). The film-cooling effectiveness trends upstream of the dilution jets are similar at each axial location irrespective of film-cooling and dilution momentum flux ratios. In addition, cooling effectiveness appears to correlate with I_{fc} and, hence, cooling mass. It is also significant to note that the increasing "sawtooth" pattern corroborates the additive nature of cooling rows in a manner consistent with superposition of effectiveness values proposed by other researchers. Similarly, just downstream of the dilution injection, at X/L = 0.43, the film-cooling momentum flux ratio of $I_{fc} = 25$ cases resulted in better surface cooling. It is interesting to note that there is a decrease just downstream of the dilution jets given that there is no film-cooling jets present (note that the hole area was included in the averages). The lateral averaged effectiveness values increased

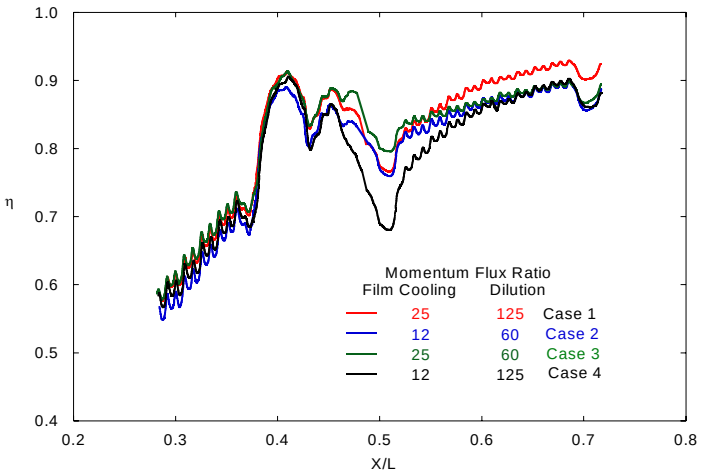

Figure 4. Lateral average of adiabatic effectiveness for all cooling configurations.

just upstream of the third panel where the film-coolant agglomerates ($0.45 < X/L < 0.48$). At $X/L = 0.5$ there is a minimum in the laterally averaged effectiveness as a result of no film-cooling holes being present. Beyond $X/L = 0.5$, the film begins to build up similar to that found upstream of the dilution hole.

Figure 4 highlights a decay in cooling effectiveness in the region between panels 2 and 3. A decay should be expected where full coverage cooling ends and/or is spatially interrupted. This is proceeded by a build up of the cooling when the next row is introduced. The effects of the dilution jets are also clear downstream of $X/L = 0.53$. In this region, the dilution jets with the higher momentum flux ratios (cases 1 and 4) show a steeper increase in the cumulative effect of cooling indicated by the adiabatic effectiveness levels, even though these two cases have different film-cooling flows. Moreover, lower local minima of effectiveness are found with the higher I_d cases. In comparison, cases 2 and 3 with the lower momentum flux ratios indicate a lower slope in the increasing effectiveness values. The lower minima and steeper slopes for cases 1 and 4 results from the fact that the higher momentum jets are more disruptive to the cooling immediately downstream of the dilution holes but produce more favorable conditions for the cooling further downstream. Since individual cooling rows are visible in the plot as give by the "sawtooth," the cooling layer has returned to a behavior typical of 'sequential row' film-cooling.

For the cases with the same momentum flux ratios of the film-cooling jets, case 3 with the lower momentum flux ratio dilution jets shows better cooling than case 1 with the higher momentum flux ratio dilution jets until $X/L = 0.55$, which is approximately 3 dilution hole diameters downstream of the dilution row. Beyond $X/L = 0.55$, the trend is reversed. This trend is similar when comparing cases 2 and 4, but the change does not occur until further downstream at $X/L = 0.63$, which is over 4 dilution hole diameters downstream. This phenomenon of film-cooling performing better for the cases with the lower momentum dilution jets is most likely due to the less disruptive nature of the low I_d jet with its lower wall-normal momentum and the reduced strength of the three-dimensional flows and turbulence energy inherent to that jet. This result is similar to Odgers and Son [7] who also indicated better cooling occurred when the film-cooling layer was interrupted by dilution jets with lower momentum flux ratios.

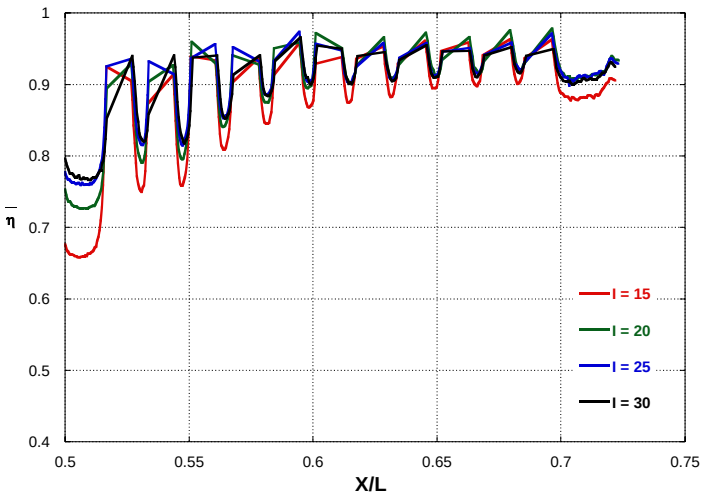

Figure 5. Adiabatic effectiveness profile for four film-cooling blowing ratios at the dilution center-line.

Because the cooling effectiveness is more dependent on film-cooling flow, a study was undertaken where the dilution flow was held constant ($I_d = 125$) and the film-cooling was varied between four different flow rates. Streamwise effectiveness line plots for these cases were generated to determine cooling effects downstream of the dilution hole centerline. From the data shown in Figure 5, it can be concluded that the adiabatic effectiveness began approaching an asymptotic value at 63% of the combustor length. The highest momentum flux ratio ($I_{fc} = 30$) was found to produce the best cooling effectiveness, but it was found that the effectiveness benefit was reduced as the blowing ratio was increased and the lowest minimum effectiveness was with the low I_{fc} cooling.

Flow and Thermal Field Measurements

The thermal fields of three planes were measured in this study as shown in Figure 6 for cases 1, 2 and 3. Focus was placed on these three flow configurations because they offered the best cooling and they allowed sufficient variation of the flow parameters. The first plane measured (1p in Figure 2) was to document the film-cooling layer approaching the row of dilution jets. It was found that cases 1 and 3 showed a higher film penetration into the freestream, which is consistent with the higher film-cooling momentum flux ratio. It can be seen from the contours in Figure 6 that the coolant accumulates up to a location of $Z/H_{in} = 0.1$ ($Z/d = 13$). It should also be noted that at the cooling hole centerline ($Y/W = 0$), the streamwise velocity at the liner wall is 2.75 times the combustor inlet velocity, as will be discussed later in the text. It was observed in the wall effectiveness contours as well as the thermal fields that the jets were discrete allowing for mainstream fluid between the hole injection locations.

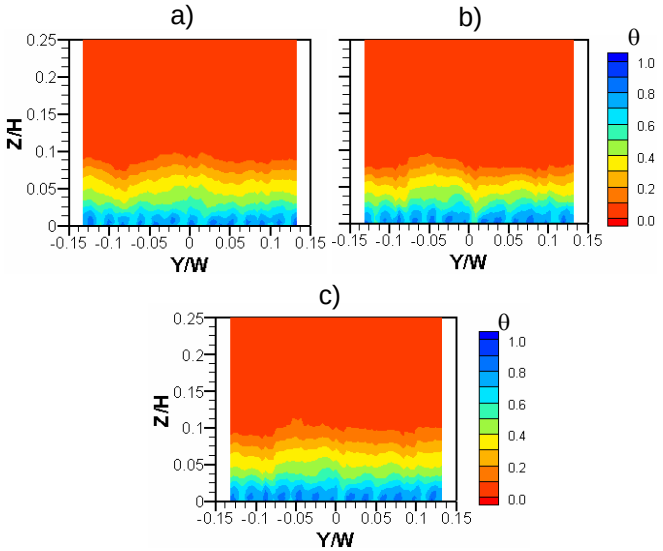

Figure 6a-c. Thermal field measurements for plane 1p in (a) case 1, (b) case 2, and (c) case 3.

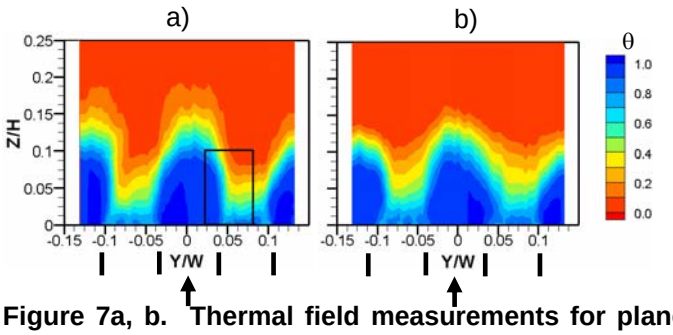

Figure 7a, b. Thermal field measurements for plane 2p for (a) case 2, (b) case 3. The black rectangle in 8a denotes where the flow field of Figure 9 was measured.

The thermal fields measured at the dilution center pitchwise location (2p in Figure 2) for cases 2 and 3 are shown in Figure 7. The penetration distance of the dilution jet core ($\theta = 0.95$) for each case was approximately 9% of the combustor height. However, there was a thicker layer of coolant between the dilution jets for case 3, whereby the flows were set at $I_{fc} = 25$ and $I_d = 60$.

The flow field measurements, shown in Figure 8a, indicate a high velocity region adjacent to the dilution jets. This high velocity region results from the film-cooling flow accelerating around the dilution jet resulting in a weak vortex at the interaction location between the dilution jet and film-cooling jet. Note that the measurement location for the flow field data in Figure 8a is indicated by the box placed in Figure 7a. Turbulence levels were also extracted from the mean and rms velocity measurements and are shown in Figure 8b. The peak turbulence level, which occured in the shear layer between the dilution jet and coolant flow, had fluctuations that were two times higher than the inlet velocity. The turbulence level at the dilution jet core was above 150%, based on the combustor inlet velocity. The mid-passage turbulence was found to be about 30%. Note that the mass-averaged velocity at this location is about 14% higher than the inlet velocity.

The velocity and turbulence fields measured at plane 1s, shown in Figure 9, is a good indication of the flow field as it approaches the dilution jet. Near the wall, velocities reach 2.5 times the inlet velocity due to the film-coolant injection. The freestream velocity reaches a maximum of 1.5 times the inlet velocity as it approaches the dilution jet. Near the wall, the film-coolant flow stagnates as it approaches the dilution jet at approximately 1% span. Upstream of the dilution jet, the turbulence level of the film-cooling layer reached a maximum of about 50% of the combustor inlet velocity. The higher turbulence level of the dilution jet core reached 150%.

The downstream thermal development of the dilution jets and the film-cooling flow for plane 3s is shown in Figure 10 for cases 1, 2, and 3. It is clear at this location that the $I_d = 125$ jet (case 1) has a penetration that is higher at 25% of the span (for the $\theta = 0.8$ contour) relative to 18% of the span for the $I_d = 60$ cases. The thermal fields indicate core values that are elliptical shaped resulting from a counter-rotating vortex pair that forms as the jets are bent by the freestream. Vakil and Thole [10] also reported a large recirculation region that extended 10% of the combustor length downstream of a dilution jet, which serves to

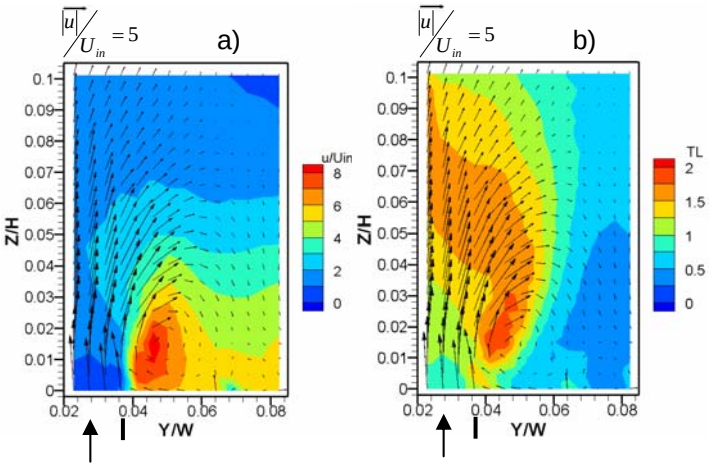

Figure 8a, b. Vectors show v/Uin and w/Uin velocity components. (a) Flow field at plane 2p for case 1 with contours showing u/Uin values. (b) Contour of turbulence level at plane 2p for case 1. Note 4x enlargement of scale.

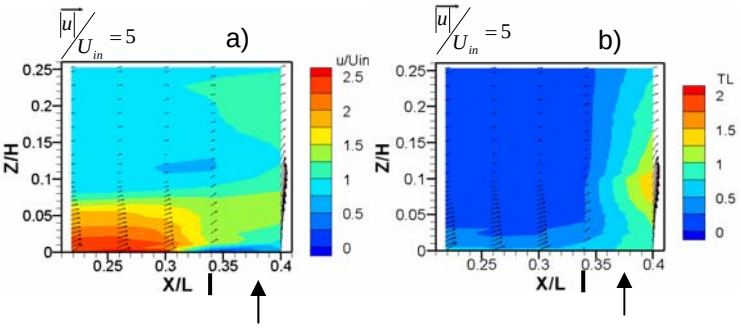

Figure 9a, b. (a) Flow field at plane 1s for case 1. Vectors show u/Uin and w/Uin velocity components and contour shows u/Uin values. (b) Flow field vectors and contour of turbulence level at plane 1s for case 1.

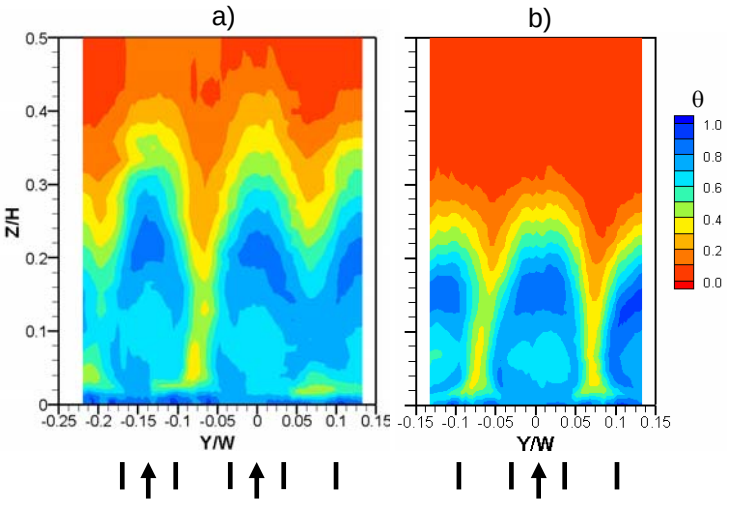

Figure 10a, b. Thermal field measurements for plane 3p for (a) case 1 and (b) case 2.

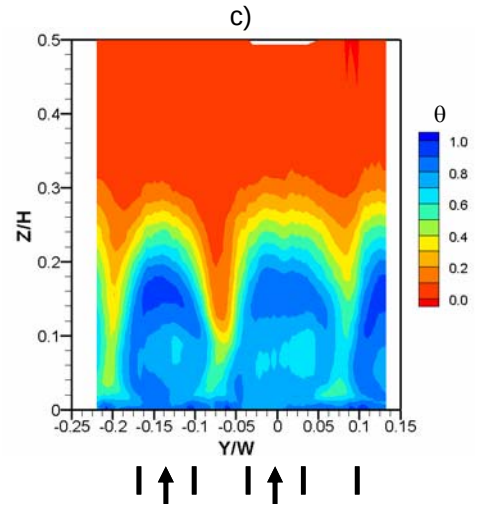

Figure 10c. Thermal field measurements for plane 3p for case 3.

recirculate warm fluid ($\theta = 0.3$) below the core of the jet.

Comparing cases 2 and 3 (Figure 10b and 10c), it is obvious there is more coolant between the dilution jets when there is more film-cooling flow injected. This observation is true from the wall to about 10% span. This confirms the conclusion that the film-cooling flow is entrained by the dilution jets and is carried off the liner wall. However, there is enough film-cooling flow for the $I_{fc} = 25$ case to ensure that there is an adequate effectiveness level at the liner surface despite the entrainment of cool flow off the wall.

CONCLUSIONS

The results of this study indicate that the cooling effectiveness for a realistic combustor wall is dependent on multiple flow mechanisms. It was important in this study to quantify the effect of the dilution jets and cooling flow, which are typical in an aero-gas turbine, on the effectiveness of the coolant at the combustor liner wall. The flow and thermal fields that these flows produced gave insight into how the coolant was transported from the film-cooling layer in the near wall region to the freestream and downstream of the dilution jets. Adiabatic effectiveness contours of the combustor wall taken using an infrared camera offer very good spatial resolution and a unique opportunity to identify hot spots and coolant streaks that develop in a representative combustor simulator.

Surface adiabatic effectiveness measurements along with thermal field measurements indicate the presence of warm fluid between the distinct film-cooling jets upstream of the dilution holes. Downstream of the dilution holes, the turbulence levels were two times higher than the local mean velocity resulting in increased spreading of the film-cooling jets. Better surface cooling resulted in the near-dilution region for the same film-cooling flows when lower momentum dilution jets were present relative to higher momentum dilution jets. The reason for this better cooling was because of the additional cooling from the interaction of the dilution jets with the combustor liner.

The flow fields indicated that the film-coolant fluid stagnates as it approaches the dilution jets. Further downstream, the film-coolant is convected around the dilution jets resulting in high streamwise velocities adjacent to the dilution jets. Turbulence measurements indicate highly localized turbulent regions that develop in the shear layer between the film-cooling jets and dilution jets. These regions partially extend into the jet cores, but remain distinct regions of high turbulence intensity. The highest turbulence regions for the dilution jets occur at the jet interfaces with the freestream flow. As such, it would be expected that good mixing would occur at these locations.

ACKNOWLEDGEMENTS

The authors gratefully acknowledge United Technologies – Pratt and Whitney for their support of this work.

REFERENCES

[1] Lefebvre, A. H., *Gas Turbine Combustion* (Taylor & Francis: Philadelphia, PA), 1999.

[2] Sasaki, M., Takahara, K., Kumagai, T., and Hamano, M., 1979, "Film Cooling Effectiveness for Injection from Multirow Holes," ASME *Journal of Engineering for Power*, Vol. 101, pp. 101-108.

[3] Andrews, G. E. and Mkpadi, M. C., 1984, "Full Coverage Discrete Hole Wall Cooling: Discharge Coefficients," ASME *Journal of Engineering for Power*, vol. 106, pp. 183-192.

[4] Andrews, G. E., Asere, A. A., Gupta, M. L., and Mkpadi, M.C., "Full Coverage Discrete Hole Film Cooling: The Influence of Hole Size," ASME 85-GT-47.

[5] Barringer, M. D., Richard, O. T., Walter, J. P., Stitzel, S. M., And Thole, K. A., 2002, "Flow Field Simulations of a Gas Turbine Combustor," *Journal of Turbomachinery*, Vol. 124, Pp. 508-516.

[6] Gritsch, M., Shulz, A., and Wittig, S., 1998, "Method for Correlating Discharge Coefficients of Film-Cooling Holes," *AIAA Journal*, vol. 36, pp. 976-980.

[7] Odgers, J. and Son, N. N., "Film Cooling—The Effect of a Cold Jet Normal to the Coolant Layer," Winter Annual Meeting, Houston, Texas, 1975.

[8] Button, B. L., "Effectiveness Measurements for a Cooling Film Disrupted by a Single Jet," 83-GT-250.

[9] Martiny, M., Schulz, A., Wittig, S. and Dilzer, M., "Influence of a Mixing-Jet on Film Cooling," 97-GT-247.

[10] Vakil, S. and Thole, K. A., 2005, "Flow and Thermal Field Measurements in a Combustor Simulator Relevant to a Gas Turbine Aero-Engine," *Journal of Engineering for Gas Turbines and Power*, vol. 127, pp. 1-11.

[11] Moffat, J. R., "Describing the Uncertainties in Experimental Results," *Experimental Thermal and Fluid Science*, Vol. 1, pp. 3-17, 1988.

[12] Holdeman, J. D., "Mixing of Multiple Jets with a Confined Subsonic Crossflow," *Prog. Energy Combust. Sci.*, Vol. 19, pp. 31-70, 1993.